Determining Performance Limits for Non-Aqueous Redox Flow Batteries

Zhijiang Tang,[†,1] Aman Preet Kaur,[†,2] Alan Pezeshki,[†,1,3] Subrahmanyam Modekrutti,[2] Frank Delnick,[1] Thomas A. Zawodzinski,[1,3] Gabriel M. Veith,*[,1] Susan A. Odom*[,2]

[1] Materials Science and Technology Division, Oak Ridge National Laboratory, Oak Ridge, TN, 37831 USA
[2] Department of Chemistry, University of Kentucky, Lexington, KY, 40506 USA
[3] Department of Chemical and Biomolecular Engineering, University of Tennessee, Oak Ridge, TN, 37996, USA

[†] These authors contributed equally to the work.

Abstract

In this work, we explore the limits of performance and energy density of a non-aqueous redox flow battery under ideal conditions. We compared the performance of an organic redox couple in a symmetric cell to that of a vanadium redox flow cell. Based on cycling performance, we expect that – when losses from separators and poor ionic conductivity are minimized – a non-aqueous flow cell operating at 3.5 V should have a 35% higher energy density than $V^{4/5+}$ couple in aqueous system at 100 mA·cm^{-2} current density for a system that could operate at 3.5 V.

I. Introduction

The development of affordable, large-scale energy storage systems is essential to enhancing the reliability and efficiency of the electrical grid to meet growing electricity demands of the rapidly evolving utilities industry. Redox flow batteries (RFBs) are one technology in use for large-scale stationary storage. One important differentiating element in considering RFBs for large-scale storage is the distinction between employing aqueous vs. non-aqueous solutions (NAqRFBs) as active electrolytes. There are various trade-offs and relative advantages or disadvantages of a given electrolyte type. We briefly outline some of the main arguments given in what follows.

Since the 1990s, all-vanadium and iron-chromium flow battery systems have been deployed on the MW/MWh level.[1–4] However, these systems, which contain aqueous electrolytes, are limited by low cell voltages and low energy densities. Specifically, the relatively narrow electrochemical

window of the water based electrolyte (1.23 to 2.5 V,[5] depending on electrode and electrolyte identity) and low solubility of transition metal redox couples (1 to 2 M transition metal in 3 to 5 M supporting electrolyte) limit energy densities to ca. 30 kWh/L for conventional operation. Nonetheless, these systems are leading the commercialization push for RFBs. In all RFBs, there is a premium on current density or power density in the stack to keep costs low by minimizing the needed area and cell count to deliver a specified power. Unlike the case for conventional batteries, energy density is of secondary importance. As members of this team have shown, well-designed aqueous all vanadium RFBs (VRBFs) are predominantly ohmically limited, and enormous improvement in current and power density is achieved by minimizing resistive losses in the cell. Aqueous RFBs benefit from relatively high proton conductivity, reaching ohmic resistances as low as ~0.1 to 0.5 $\Omega \cdot cm^2$, with the former limit being approached in some studies resulting in high performance at steady state and upon cycling.

NAqRFBs, especially those containing organic electro-active components, offer an opportunity to design batteries that possess higher energy densities and are more cost effective than their aqueous peers.[6] Compared to the limited voltages of aqueous RFBs, the operational voltage of NAqRFBs can be extended to at least 4 V by utilizing electrolytes with larger electrochemical windows (e.g. the window for acetonitrile containing 0.1 M TEABF$_4$ is 4.3 V).[5] Moreover, the flexibility in choice of solvent and supporting electrolyte in NAqRFBs allows for the consideration of a large variety of metal-free redox couples. Metal-ligand complexes and metal-free organic redox couples are two major types of redox couples being investigated in NAqRFBs.[7]

Although the solubility of metal-ligand redox species can be enhanced by ligand selection, the solubility of most reported metal-ligand complexes is severely limited in organic solvents.[7] By contrast, organic redox couples can reach significantly higher solubility. For example, a 7 M solution of quinoxaline can be realized in propylene carbonate.[8] Also, some of the more highly soluble derivatives evaluated as flow battery candidates are liquids, including derivatives of dialkoxybenzene,[9] TEMPO,[10] phenothiazine,[11] and quinone.[12] Less soluble organic compounds can often be easily modified, providing an opportunity to raise the energy density of electrolytes. Another approach to raising energy densities involves the utilization of organic compounds that undergo multiple electron-transfer reactions (e.g. phenothiazines, quinones[13,14] and quinoxalines[8]). Moreover, the ability to tune the molecular structure of organic compounds enables redox potentials to be shifted such that the full electrochemical window of an electrolyte solution may

be utilized. Finally, organic redox couples may provide a pathway to lower-cost electrolytes, since their utilization can eliminate the use of metal-based components.[15] With the potential to provide 5 to 6 M of transferable electrons in organic solvents and a working voltage of 4 V, a theoretical energy density of 300 Wh·L^{-1} can be envisioned for non-aqueous RFBs, which is about 10x higher than aqueous vanadium systems.

Despite the potentially higher energy densities of NAqRFBs, no system has been commercialized. Poor ionic conductivity, low solubility and/or stability of many available redox species, and the limited performance of available membranes and separators has hindered the development of non-aqueous systems. The combination of these limitations presents a challenge, as a system containing one improved component may fail as rapidly as an equivalent without the same improvement if another component is limiting the performance. In this work, we sought to identify a maximum expected performance, assuming that all the problems outlined above are solved. To accomplish this task, we studied the performance of an organic redox couple in a no-gap battery cell architecture.[16] A symmetric cell configuration was used to evaluate the performance of the neutral / radical-cation redox couple of a phenothiazine derivative.[17,18] We directly take on the power/energy density trade-off by working in a non-aqueous electrolyte with relatively high conductivity. In this way, we can estimate the highest current density that might be achievable with the presently available electrolytes. This will put the NARFB approach in its most favorable light.

II. Experimental

General

Unless specified, materials were used as received. Acetonitrile (ACN, 99.9%, extra dry over molecular sieves) was purchased from Acros Organics and was opened in an argon-filled glove box. Tetraethylammonium tetrafluoroborate (TEABF$_4$, 99%) was obtained from Alfa Aesar, which was further recrystallized from ethanol, vacuum dried, and stored inside the glove box prior to use in RFB experiments. The trilayer separator 2325 was provided by Celgard. SGL GFD3

carbon felt electrodes were purchased from the SGL Carbon Group. Cell hardware and graphite flow fields were obtained from Fuel Cell Technologies, Inc.

Synthesis and Electrolyte Preparation

N-ethylphenothiazine (EPT) and its tetrafluoroborate radical cation salt (EPT-BF$_4$) were synthesized as previously reported.[11] Three solutions were prepared for electrochemical analysis. Each solution's components are listed below.

Solution A: 0.04 M EPT, 0.04 M EPT-BF$_4$, and 1.00 M TEABF$_4$ in ACN

Solution B: 0.08 M EPT and 1.00 M TEABF$_4$ in ACN

Solution C: 0.08 M EPT-BF$_4$ and 1.00 M TEABF$_4$ in ACN

Flow Cell Construction

The 5 cm^2 active-area flow cell was built with a no-gap architecture, assembling it with the separator sandwiched between two carbon felt electrodes, which were compressed to ~70% of their original thickness when stacked. The single-channel serpentine graphite flow fields were assembled as reported previously.[16] Testing was carried out in an argon-filled glovebox. Prior to use, the cell was flushed with ACN to remove potential impurities. Cartridge heaters connected to an Omega CSC32 temperature controller were used to maintain cell temperature at 30 ºC. The electrolyte solution was pumped into the cell through ChemDurance tubing using a MasterFlex L/S peristaltic pump. (See Figure S1 for a drawing of the setup.)

Electrochemical Analysis

Electrochemical measurements were carried out with a Bio-Logic Instruments SP-240 potentiostat with a 4 A booster. For all experiments, cells were operated in two-electrode configuration. To obtain the first polarization curve, electrochemical analysis was performed as Solution A (80 mL) was pumped through both sides of the cell using a single hydraulic circuit at a flow rate of either 20 or 50 mL/min.

The cycling experiment was conducted at a current density of 100 mA/cm^2. Solution B and Solution C (50 mL of each) were recirculated through the cell (on opposite sides) at 50 mL/min.

Initially, electrons flowed from Solution B to Solution C until the cell voltage reached 0.45 V. Then, the current direction was switched until the cell voltage reached -0.45 V. Cycling continued in a similar manner thereafter until no current could be passed. Afterward, the two solutions were combined, and a second set of polarization curves was recorded as the resultant solution was passed through both sides of the cell that contained used separator and electrodes at 50 mL/min flow rate.

Polarization curves and AC impedance spectra were obtained using staircase potentiostatic electrochemical impedance spectroscopy. Current and AC impedance spectra of the battery were recorded after a set voltage was superimposed across the cell. A series of measurements was conducted to complete a polarization curve measurement at a designated voltage increment. The high frequency resistance (HFR) was taken as the high frequency intercept of the impedance curve with the real axis. Area specific resistance (ASR) was obtained by correcting HFR to active area of battery cell (5 cm^2). IR correction was carried out by compensating ohmic voltage loss to overall cell voltage as:

$$E_{corrected} = E_{measured} - I \times R$$

UV-Visible Spectroscopy
All samples were prepared in dry ACN. For the fresh radical cation sample, a stock solution was prepared by dissolving EPT-BF$_4$ (6.28 mg, 0.02 mmol) in ACN (5 mL) to obtain a concentration of 4×10^{-3} M. An aliquot of the stock solution was taken and further diluted to achieve a concentration of 1.5×10^{-4} M. Similarly, an aliquot of the cycled solution with initial concentration of 4×10^{-2} M in radical cation (considering 50:50 mix of EPT and EPT-BF$_4$) was diluted to achieve a radical cation concentration of 1.5×10^{-4} M, equivalent to the concentration of a freshly prepared solution of radical cation. A stock solution of neutral EPT was prepared by dissolving EPT (0.91 mg, 4.0×10^{-3} mmol) in ACN (20 mL) and was diluted to obtain a concentration of 1.5×10^{-4} M. All measurements were carried out on an Agilent 8453 diode array spectrophotometer within 15 min of sample preparation.

III. Results and Discussion
In a full cell test with two redox couples, a charging step involves the redox couple "A" in the negative half of the cell (the anolyte) accepting an electron, creating radical anion "A·⁻", and the

redox couple "C" on the other half (the catholyte) donating an electron, becoming radical cation "C$^+$" (Figure 1, left). In the discharge step, the process is reversed, again creating "A" and "C". In this work, only one redox couple is involved. One compartment begins with neutral "C", and in a charging step, becomes "C$^+$". The other compartment contains "C$^+$", which is reduced to "C" during the first step (Figure 1, right). In other words, in each step of the cycle, the symmetric cell switches from C/C$^+$ to C$^+$/C. The charge moves from one half of the cell to the other, creating the mirror image of its starting point in each half cycle (if a 'full cycle' involves both charge and discharge). The analysis of an electrolyte solution of interest is simplified in the symmetric cell, as there is no convolution of performance characteristics from a differing chemical species as would be the case in a full cell battery. In addition, because there is no possibility of cross-contamination, the separator requirements are much simpler.
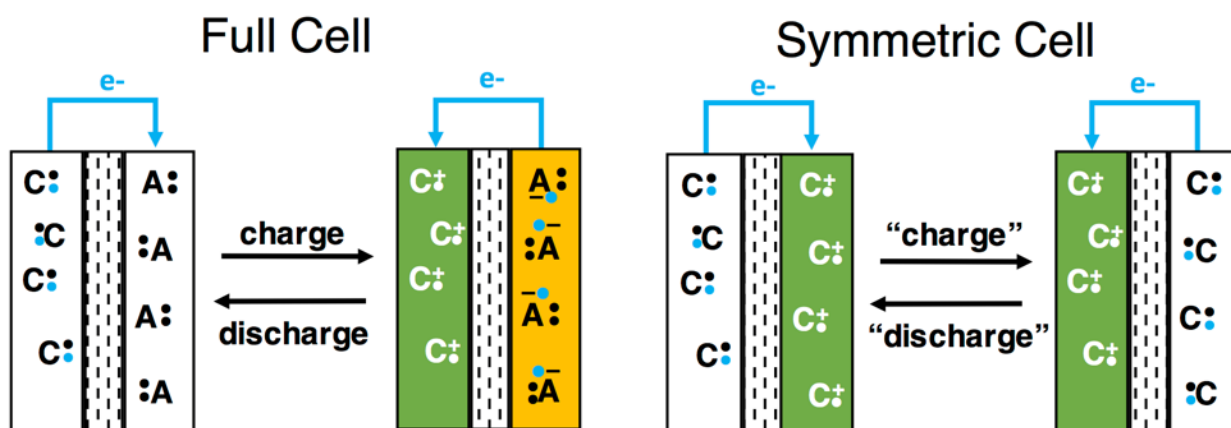

Figure 1. Representation of charge and discharge processes in a full cell (left) and in a symmetric cell (right). In a full cell, C donates electrons to A during charge. In a symmetric cell, charge is moved from a neutral species to its oxidized form. Note that the terms "charge" and "discharge" do not truly apply to a symmetric cell, but are rather used to describe the movement of charge from one half of a cell to the other.

To measure optimal performance of an organic redox couple in a non-aqueous environment, maximization of redox couple lifetime and minimization of ohmic losses were considered. For the redox couple, *N*-ethylphenothiazine (EPT) and its tetrafluoroborate radical-cation salt (EPT-BF$_4$) were chosen. The robust nature of this redox couple was expected to allow extensive cycling.[11,19]

Tetraethylammonium tetrafluoroborate (TEABF$_4$) in acetonitrile (ACN) was chosen as the supporting electrolyte because its conductivity is one of the highest reported values among the commonly used non-aqueous electrolytes (26.3 mS·cm^{-1} with 1 M TEABF$_4$).[197] Additionally, we expected that the low viscosity of ACN (0.34 cP) would facilitate convective mass transport, thus minimizing mass transport resistance. For cell cycling, 0.08 M was chosen for the total concentration of redox couple, a value lower than the solubility limits of both EPT and EPT-BF$_4$ in the electrolyte. Celgard 2325 was chosen as the separator to minimize ohmic losses as much as possible. While this separator would likely be unsuitable for full cell operation due to crossover, it is suitable for symmetric cell experiments where cross-contamination cannot occur.

Before performing cell cycling experiments, polarization curves were obtained to determine the best possible performance of the catholyte for later comparison with cycled electrolyte. A solution containing a 1:1 ratio of EPT:EPT-BF$_4$ (both at 0.04 M in 1.00 M TEABF$_4$/ACN for 0.08 M total concentration of the redox couple; Solution A) was circulated on both sides of the flow cell to model catholyte at 50% state of charge (SoC). By performing these experiments prior to cycling, we are able to benchmark the performance prior to any membrane fouling, precipitation, or other factors that would lead to limitations in cell performance. Because the solutions passing through the electrodes were equivalent, we expected each half-cell to contribute similar amounts of overpotential.[17,18] Polarization curves recorded at flow rates of 20 and 50 mL/min[1] are shown in Figure 2a. For comparison, polarization curves for V^{2+}/V^{3+} and V^{4+}/V^{5+} redox couples, both at 0.1 M in 5 M H$_2$SO$_4$ (aq), in the equivalent setup are shown in the same plot.[20] It is important to say that working at 0.1 M radically understates the performance of a practical vanadium system, in which concentrations of 1.5 to 2.0 M are utilized; we chose to conduct these lower concentration experiments to provide a better comparison to the performance of EPT/EPT$^+$ cells.
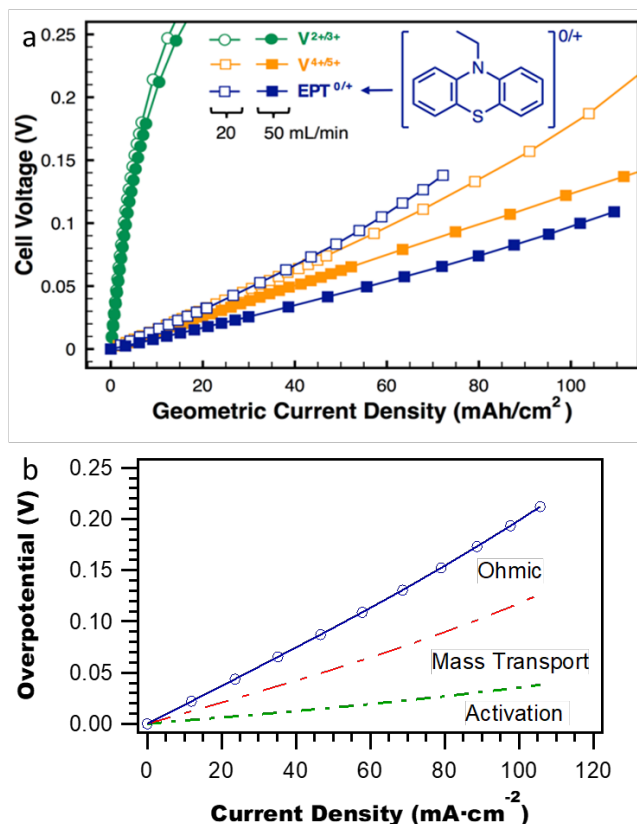
Figure 2. (a) iR-corrected cell polarization curves of the EPT/EPT$^+$ couple at 0.08 M in 1.00 M TEABF$_4$/ACN (blue) and of the V$^{2/3+}$ (green) and V$^{4/5+}$ (orange) couples each at 0.1 M in 5 M H$_2$SO$_4$ (aq), all at 50% SoC. (b) Quantitative analysis of contributions of ohmic, mass transport and activation overpotential losses to the overall polarization loss of 0.08 M EPT/EPT$^+$ couple at 50% SoC in 1.00 M TEABF$_4$/ACN, at a circulation rate of 50 mL/min[1].

Figure 2a compares the phenothiazine (EPT$^{0/+}$) and vanadium (V$^{2+/3+}$ and V$^{4+/5+}$) redox couples. The V$^{2+/3+}$ couple, which has reaction kinetics about 40 times slower than the V$^{4+/5+}$ couple in aqueous V RFBs,[21,22] shows the most overpotential, with the highest cell voltages observed at low current densities. At flow rates of 20 and 50 mL/min[1], the cell voltages and trends for the EPT$^{0/+}$ couple were remarkably similar to the V$^{4+/5+}$ couple, with the EPT$^{0/+}$ couple having slightly higher voltages at the slower flow rate and slightly lower values at the faster flow rate. The slopes for both couples remain largely linear over the measured current densities. At a current density of 100 mA/cm^2, the IR-corrected overpotential loss of the EPT$^{0/+}$ couple is 90 mV, while that for the V$^{4/5+}$ couple is higher at 110 mV. Considering that the concentration of EPT is 25% lower than vanadium system, in this comparison, the current density output per overpotential penalty of the EPT$^{0/+}$

couple is roughly 35% higher than that of the $V^{4/5+}$ couple at 100 mA/cm^2. In a practical VRFB system with 1.7 M vanadium at the same flow rate, the positive electrode, negative electrode, and IR can cause 13, 20, and 26 mV overpotential at 100 mA/cm^2.[20] Thus, in a hypothetical system with more than 1 M EPT$^{0/+}$, the corresponding electrode overpotential is expected to be lower than 10 mV at 100 mA/cm^2.

While the complex impedance spectra were not fitted to a macrohomogeneous porous electrode model, qualitative and semi-quantitative conclusions can be drawn following the approach by Pezeshki and co-workers.[17] The spectra (Figure S3) include both high and low frequency features. The high frequency feature can be attributed to a combination of liquid electrolyte resistance through the porous electrode as well as charge transfer resistance. This high frequency feature was approximately 0.3 Ωcm^2. The low frequency feature can be attributed to mass transport resistance; the sensitivity of this feature to flow rate confirms that it is related to mass transport. The open-circuit mass transport resistances were estimated 1.8 and 0.7 Ωcm^2 at 20 and 50 mL/min^1, respectively. The high-frequency intercept is an ohmic resistance and includes contributions from the ionic resistance through the separator and the liquid electrolyte and was 0.85 Ωcm^2 at 100 mA/cm^2. Overall, mass transport and ohmic resistance are both limiting factors for the EPT redox couple, while the charge transfer process is facile and non-limiting.

To better deconvolute the contribution of activation, ohmic, and mass transport resistance to overall overpotential loss in pseudo battery, AC impedance spectra were recorded across the whole cell at varying overvoltages at a flow rate of 50 mL/min^1 (Figure S4). The corresponding overpotential caused by each factor, shown in Figure 2b, were calculated using a previously reported method.[22,23] The results of these calculations affirm that ohmic and mass transport resistances are the major contributing factors to observed overpotentials. At 100 mA/cm^2, ohmic and mass transport contribute roughly 80 mV to the overpotential, in comparison to 0.34 mV from electrode activation. The solvent ACN, with a viscosity of 0.34 cP, provides a near-best case scenario among the non-aqueous solvents used in batteries, as does the use of the Celgard separator, as the combination of Celgard separator with TEABF$_4$/ACN has been reported to provide one of the lowest internal resistance values among evaluated separator(membrane)/nonaqueous electrolyte combinations.[6,24,25] Thus, it should be noted that the

mass transport may be hindered when more viscous solvents and higher salt concentrations are utilized, and the resistance may be higher if the separator is replaced with a membrane. Although the IR of the symmetric battery (0.81 Ωcm^2) was about 2-3x higher than that of high performing VRFB system (0.3 Ωcm^2),[17] ohmic losses can potentially be offset by running NAqRFBs at higher voltages.

For cycling experiments, solutions containing both 0.08 M EPT and 0.08 M EPT-BF$_4$ were employed, which corresponds to a theoretical capacity of 386 coulombs for each solution. The capacity measured in the first cycle was 232.7 coulombs (60.3% of the theoretical capacity), which – assuming negligible cross-over – corresponds to a SoC range in each reservoir from 19.9 to 80.2%. Using these values for the range of SoC, we can calculate the open circuit voltage (OCV) using the following equations:

$$E_{cell} = E_{R1} - E_{R2}$$

$$E_{cell} = \frac{RT}{F}\left(\ln\left(\frac{[\text{EPT}_1^+]}{[\text{EPT}_1]}\right) - \ln\left(\frac{[\text{EPT}_2^+]}{[\text{EPT}_2]}\right)\right)$$

$$E_{cell} = \frac{RT}{F}\left(\ln\left(\frac{SoC_1[\text{EPT}_{T1}]}{(1 - SoC_1)[\text{EPT}_{T1}]}\right) - \ln\left(\frac{SoC_2[\text{EPT}_{T2}]}{(1 - SoC_2)[\text{EPT}_{T2}]}\right)\right)$$

$$E_{cell} = \frac{RT}{F}\left(\ln\left(\frac{SoC_1\,(1 - SoC_2)}{(1 - SoC_1)\,SoC_2}\right)\right)$$

where the subscripts 1 and 2 refer to the two reservoirs and refers to the total concentration of EPT in each reservoir. At 303 K, a 60.3% capacity utilization leads to 72.9 mV for the OCV, not far from the measured value for the first cycle of 73.2 mV. The close agreement between the capacity-predicted OCV and the actual open circuit voltage indicates that the net effect of crossover is near zero.

Due to overpotential loss and designated potential window limit during battery operation, the theoretical battery capacity can only be partially utilized. Active species crossover is also a common problem that lowers the coulombic efficiency (CE). However, the degree of crossover

cannot be evaluated by CE in the scope of this work, due to the cell's symmetry. Given that the open circuit voltage after cycle 1 is 73.2 mV, while the cell voltage at the end of the cycle is 450 mV, the total cell polarization is ~380 mV. The first-cycle ASR was 1 Ωcm^2, and with a current density of 100 mA/cm^2, the ohmic overpotential through the electrolyte was 100 mV. Thus, based on the polarization curve analysis, the majority of 280 mV IR corrected overpotential was to be associated with concentration polarization and mass transport losses, including electrolyte related pseudo-IR losses through the electrodes. While these losses are directly derived from the ionic resistance of the electrolyte as it relates to transport of ionic reactive species into and out of the electrode, this loss is undetected by ASR measurements. The electrode is electronically shorted yet ionic resistance decreases the electrochemical potential locally through the electrode. The result is a residual linear characteristic of the polarization curve after IR correction is carried out using the value from an ASR measurement. This behavior is consistent with the shape of the curves shown in Figure 2, with upward curvature most likely associated with concentration polarization for the low flow rate cases.

Figure 3 shows the capacity and ASR values, both vs. cycle number (Figure 3a) or vs. time (Figure 3b) for cells cycled at a current density of 100 mA/cm^2 and a flow rate of 50 mL/min. Initially, over 60% of theoretical battery capacity was utilized in the first full cycle. However, the cell eventually lost all capacity due to increased ohmic resistance and ineffective performance of the electrode. The capacity retention of the cell remained relatively stable over the first 200 cycles (56 h), with only 7.7% capacity loss, falling from 232.7 coulombs to 215.1 coulombs. The initial stability in cycling is consistent with high stability of the EPT redox couple in the battery electrolyte environment. However, after 200 cycles, the capacity of the battery decreased more rapidly, eventually falling to less than 1% of its original capacity after 800 cycles. The increase in ohmic resistance is the main reason for the decline in measurable capacity, as evidenced by changes in the cell's ASR: From cycle 200 to 800, the ASR increased from 1.38 to 2.93 Ωcm^2. Accordingly, the associated ohmic overpotential increased to 0.293 V. Because the ionic conduction in Celgard occurs in electrolyte solution wicked into the pore structure, the increased ohmic overpotential is likely caused by pore clogging or dewetting of the Celgard separator.
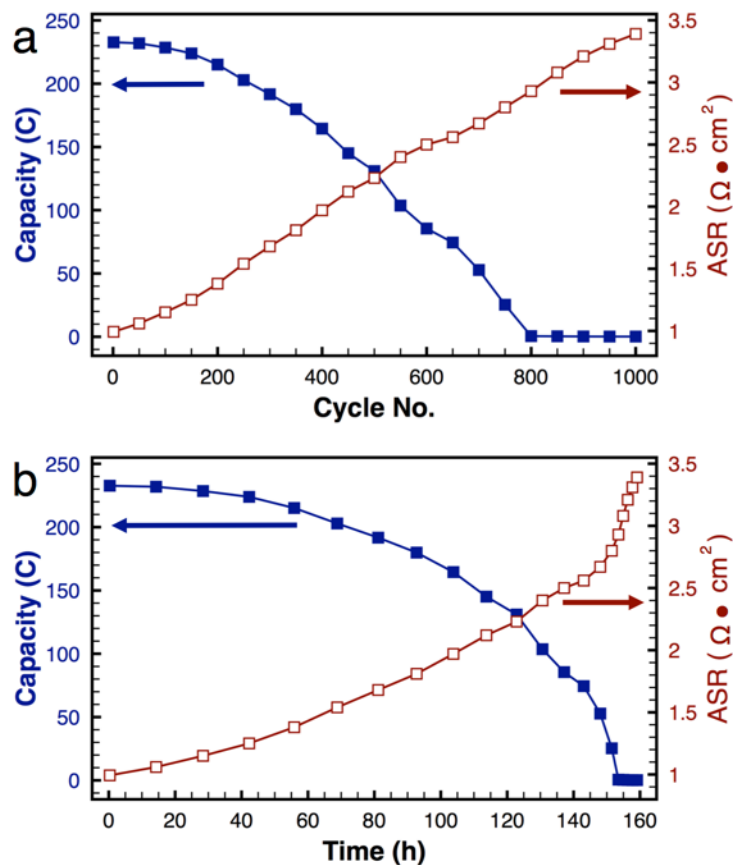
Figure 3. Capacity and area specific resistance (ASR) vs. cycle number (a) or time (b).

Compared to equivalent uncycled solutions, higher voltages in the iR-corrected polarization curves of the combined cycled electrolyte solutions (Figure 4a) indicate significant increase in electrode polarization loss. For 20 mL/min, a 50% increase was observed at 68 mA/cm^2. For 50 mL/min, a 64% increase was observed at 87 mA/cm^2. The increasing slope at higher current densities for post- vs. pre-cycled solutions indicates that the characteristics of the post-cycled solutions are dominated by mass transport. Possible causes for these changes include reduced species concentration in solution or physical changes in the electrode that lead to more tortuous diffusion pathways or reduced surface area, such as precipitation of salts from the electrolyte or deposition of EPT degradation products. Analysis of cycled solutions, as discussed below, suggests that little to no degradation of EPT occurred; therefore, it is likely that a physical change in the electrode, rather than a change in active species concentration, caused the increased mass transport polarization.
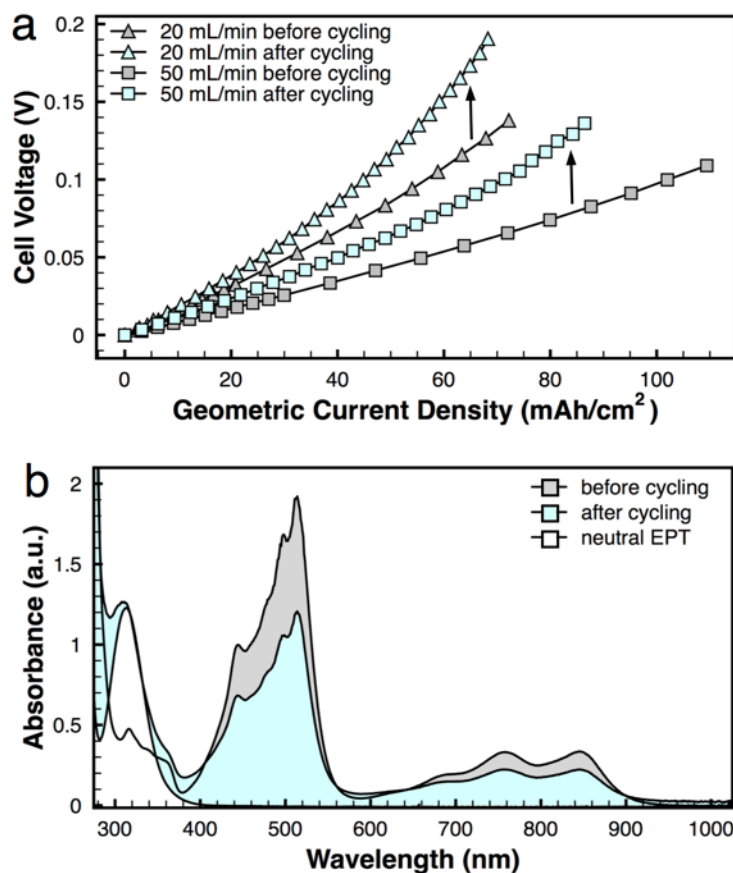
Figure 4. (a) iR-corrected polarization curves of the solutions before and after cycling at 100 mA/cm^2 at flow rates of 20 or 50 mL·min^{-1}. (b) UV-vis absorption spectra of solutions of a freshly prepared EPT-BF$_4$ (grey), EPT-BF$_4$ after cycling experiments (blue), and neutral EPT (white).

We analyzed a diluted solution of the cycled electrolyte using UV-vis absorption spectroscopy to determine what components were present. The absorption spectrum (Figure 4b) is consistent with previous spectra of EPT radical cations[26–28] and, from 400-1100 nm, matches the features of a freshly prepared solution of EPT-BF$_4$ at the same concentration as the diluted cycled solution, if no decomposition had occurred during cycling. The difference in peak intensities indicates approximately a 2:3 ratio of radical cation concentration in the cycled:fresh solutions. An additional peak at ca. 315 nm in the cycled solution corresponds to neutral EPT. Thus, while it is possible that decomposition occurred during cycling, if so, the products are not evident in the electrolyte solution. In combination with ASR results, the UV-vis results support that fouling of the membrane is the likely the major cause of the observed capacity fade.

IV. Conclusions

The facile reaction kinetics and mass transport of EPT and its radical cation in a symmetric cell provide evidence to support the use of phenothiazine derivatives as positive electrolytes in NAqRFBs. The current densities observed here are among the highest reported for NAqRFBs. While a more soluble, higher potential redox couple than EPT/EPT$^+$ is needed for cells with realistic energy densities, we have shown that molecular modification can increase both of these values. Our results show that if an OCV of 3.5 V can be achieved at 50% SoC, with redox couples possessing equally facile charge transfer and mass transport, that we expect to be able to achieve a voltage efficiency of approximately 86% when operating at 100 mA/cm^2. While we have shown that solubility and redox potentials of phenothiazines can be increased through molecular modification, challenges exist in identification of an equivalently soluble, stable negative redox couple. Furthermore, for small molecules like EPT, no commercial membranes with high selectivity and low resistance exist. Lastly, irrespective of the specific materials used in this study, our results highlight the importance of deconvoluting the contributors to resistance, as this knowledge can be used to inform the selection of more optimal flow cell components.

Reference

(1)   Chen, H.; Cong, T. N.; Yang, W.; Tan, C.; Li, Y.; Ding, Y. *Prog. Nat. Sci.* **2009**, *19*, 291–312.

(2)   Skyllas-kazacos, M.; Kazacos, G.; Poon, G.; Verseema, H. *Int. J. Energy Res.* **2010**, *34*, 182–189.

(3)   Chen, J.; Xu, Z.; Li, B. *J. Power Sources* **2013**, *241*, 396–399.

(4)   Shibata, T.; Kumamoto, T.; Nagaoka, Y.; Kawase, K. *SEI Tech. Rev.* **2013**, *76*, 14–22.

(5)   Bard, A. J.; Faulkner, L. R. *Electrochemical Methods Fundamentals and Applications*.

(6)   Huang, Y.; Gu, S.; Yan, Y.; Li, S. F. Y. *Curr. Opin. Chem. Eng.* **2015**, *8*, 105–113.

(7)   Gong, K.; Fang, Q.; Gu, S.; Li, S. F. Y.; Yan, Y. *Energy Environ. Sci.* **2015**, *8*, 38–49.

(8)   Brushett, F. R.; Vaughey, J. T.; Jansen, A. N. *Adv. Energy Mater.* **2012**, *2*, 1390–1396.

(9)   Huang, J.; Cheng, L.; Assary, R. S.; Wang, P.; Xue, Z.; Burrell, A. K.; Curtiss, L. A.;
        Zhang, L. *Adv. Energy Mater.* **2015**, *5*, 1–6.

(10)   Wei, X.; Xu, W.; Vijayakumar, M.; Cosimbescu, L.; Liu, T.; Sprenkle, V.; Wang, W. *Adv.
        Mater.* **2014**, *26*, 7649–7653.

(11)   Milshtein, J. D.; Kaur, A. P.; Casselman, M. D.; Kowalski, J. A.; Modekrutti, S.; Zhang,
        P. L.; Harsha Attanayake, N.; Elliott, C. F.; Parkin, S. R.; Risko, C.; Brushett, F. R.;
        Odom, S. A. *Energy Environ. Sci.* **2016**, *9*, 3531–3543.

(12)   Shimizu, A.; Takenaka, K.; Handa, N.; Nokami, T.; Itoh, T.; Yoshida, J. I. *Adv. Mater.*
        2017, *29*, 1–5.

(13)   Lin, K.; Chen, Q.; Gerhardt, M. R.; Tong, L.; Kim, S. B.; Eisenach, L.; Valle, A. W.;
        Hardee, D.; Gordon, R. G.; Aziz, M. J.; Marshak, M. P. *Science* **2015**, *349*, 1529–1532.

(14)   Huskinson, B.; Marshak, M. P.; Suh, C.; Er, S.; Gerhardt, M. R.; Galvin, C. J.; Chen, X.;
        Aspuru-Guzik, A.; Gordon, R. G.; Aziz, M. J. *Nature* **2014**, *505*, 195–198.

(15)   Zhang, M.; Moore, M.; Watson, J. S.; Zawodzinski, T. A.; Counce, R. M. *J. Electrochem.
        Soc.* **2012**, *159*, A1183–A1188.

(16)   Aaron, D. S.; Liu, Q.; Tang, Z.; Grim, G. M.; Papandrew, A. B.; Turhan, A.; Zawodzinski,
        T. A.; Mench, M. M. *J. Power Sources* **2012**, *206*, 450–453.

(17)   Pezeshki, A. M.; Sacci, R. L.; Delnick, F. M.; Aaron, D. S.; Mench, M. M. *Electrochim.
        Acta* **2017**, *229*, 261–270.

(18)   Darling, R. M.; Perry, M. L. *ECS Trans.* **2013**, *53*, 31–38.

(19)   Odom, S. A.; Ergun, S.; Poudel, P. P.; Parkin, S. R. *Energy Environ. Sci.* **2014**, *7*, 760–
        767.

(20)   Tang, Z.; Elgammal, R.; Pezeshki, A.; Browning, K.; Helmreich, G.; Veith, G.; Mench,
        M.; Zawodzinski, T. In *229th ECS Meeting*; 2016; p 383.

(21)   Aaron, D.; Sun, C. N.; Bright, M.; Papandrew, A. B.; Mench, M. M.; Zawodzinski, T. A.

ECS Electrochem. Lett. **2013**, *2*, A29–A31.

(22)   Sun, C. N.; Delnick, F. M.; Aaron, D. S.; Papandrew, A. B.; Mench, M. M.; Zawodzinski, T. A. *ECS Electrochem. Lett.* **2013**, *2*, A43–A45.

(23)   Sun, C. N.; Delnick, F. M.; Aaron, D. S.; Papandrew, A. B.; Mench, M. M.; Zawodzinski, T. A. *J. Electrochem. Soc.* **2014**, *161*, A981–A988.

(24)   Su, L.; Darling, R. M.; Gallagher, K. G.; Xie, W.; Thelen, J. L.; Badel, A. F.; Barton, J. L.; Cheng, K. J.; Balsara, N. P.; Moore, J. S.; Brushett, F. R. *J. Electrochem. Soc.* **2016**, *163* (1), A5253–A5262.

(25)   Hudak, N. S.; Small, L. J.; Pratt, H. D.; Anderson, T. M. *J. Electrochem. Soc.* **2015**, *162*, A2188–A2194.

(26)   Narayana, K. A.; Casselman, M. D.; Elliott, C. F.; Ergun, S.; Parkin, S. R.; Risko, C.; Odom, S. A. *ChemPhysChem* **2015**, *16*, 1179–1189.

(27)   Poudel, P. P.; Ergun, S.; Parkin, S. R.; Odom, S. A. *Preprints – American Chemical Society, Division of Energy & Fuels* (2013) 58, 108–109.

(28)   Ergun, S.; Elliott, C. F.; Kaur, A. P.; Parkin, S. R.; Odom, S. A. *J. Phys. Chem. C* **2014**, *118*, 14824–14832.

Determining Performance Limits for Non-Aqueous Redox Flow Batteries

## I. Flow Battery Setup
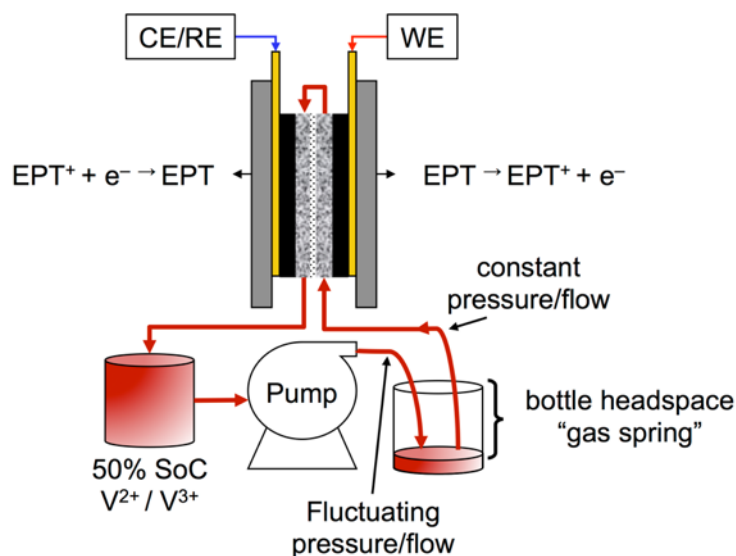
Figure S1. Diagram representing the symmetric flow cell setup utilized in this study.

II. Cyclic Voltammetry

Cyclic voltammetry was performed in symmetric battery setup as described in experimental section without electrolyte circulation. The test was carried out on one electrode as working electrode, while the other side serving as both counter electrode and reference electrode. The scan rate was 5 mV/s.
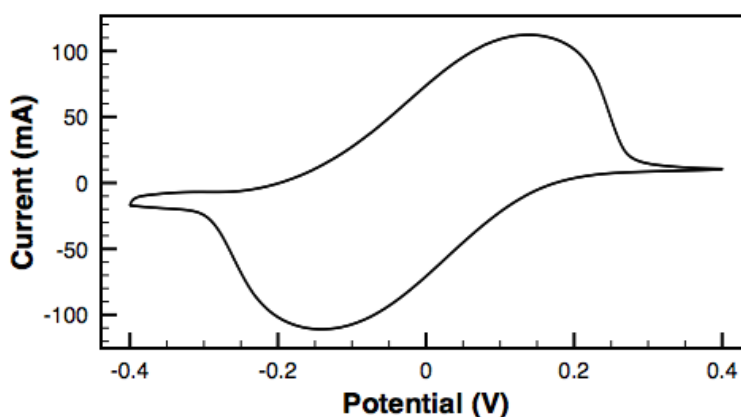

Figure S2. Cyclic voltammogram of EPT of 0.08 M in 1.00 M TEABF$_4$ in ACN on SGL GFD3 carbon felt electrodes at 5 mV/s in symmetric cell.

III. Impedance Spectroscopy

AC impedance measurements were carried out on symmetric battery with electrolyte circulated at 20 or 50 mL/min (Figure S3). The sinusoidal AC perturbation of 5 mV altitude was superimposed on the cell at 0 V which is open circuit voltage. The frequency of the measurement ranged from 1 MHz to 60 mHz. To investigate the impedance response of the symmetric cell at varying overvoltages, an AC impedance spectrum was recorded from 0 to 0.2 V overvoltage (Figure S4).
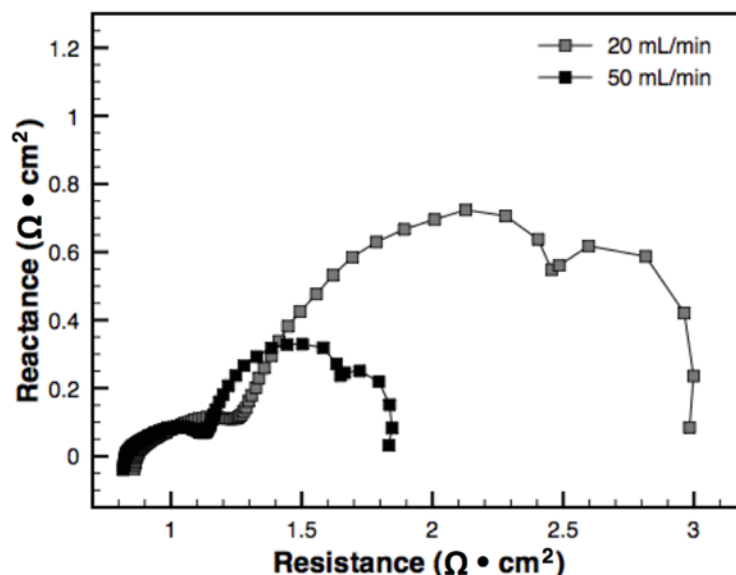
Figure S3. The AC impedance spectra of the symmetric battery with 0.08 M EPT of 50% SoC in ACN with 1.00 M TEABF$_4$ with electrolyte circulation at 20 or 50 mL/min.
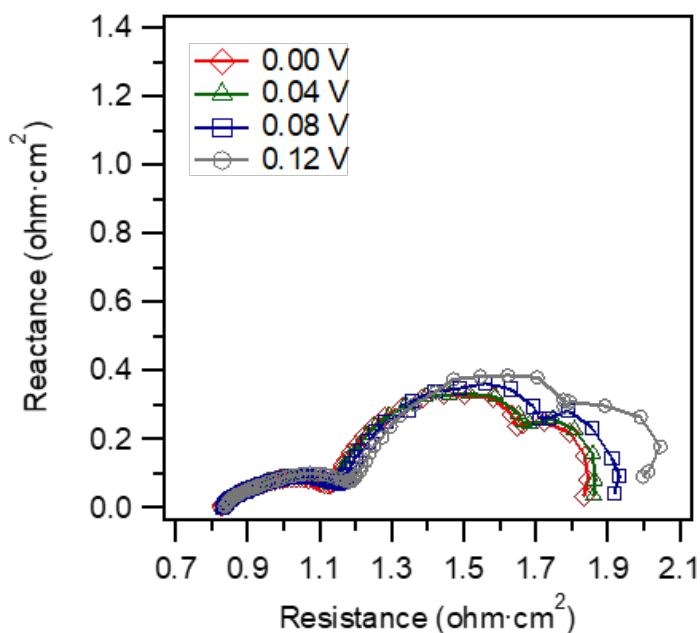
Figure S4. The AC impedance spectra of the symmetric battery with 0.08 M EPT of 50% SoC in ACN with 1.00 M TEABF$_4$ with varying overvoltage with an electrolyte flow rate of 50 mL/min.